ORIGINAL PAPER

Beverloo law for hopper flow derived from self-similar profiles

Fernando Alonso-Marroquin[1] · **Peter Mora**[2]

Received: 8 February 2020 / Accepted: 7 October 2020 / Published online: 26 November 2020

Abstract
We use particle simulations to investigate the mass flow in two-dimensional hopper flow and to analyze the dependency of the flow rate with the bottleneck width and the particle diameter. A flow rate law is derived from self-similar velocity and density profiles at the neck. The resulting relation is an enhancement of the Beverloo relation that incorporates the dependency of the density with the neck width. The parameters of the Beverloo relation are interpreted by coupling the hourglass theory with the free-fall arch theory using non-zero arch velocity as accounted by the hourglass theory.

Keywords Granular flow · Beverloo relation · Hopper flow · Hourglass theory

1 Introduction

The description of the two-dimensional flow of particles through bottlenecks has been instrumental in the understanding of granular flow in conveyor belts [1], pedestrian flow [10], sheep flow [8], and flow of other complex biological entities [23]. Observations of the flow rate when the diameter of the bottleneck is a few times the particle diameter have raised some questions about the applicability of the widely used Beverloo relation near the regime of intermittent flow [11, 12, 14, 16].

For gravity-driven flow, the hourglass theory (HGT) has been used the explain the Beverloo relation [15].

The theory predicts that the mass flow rate scales with the diameter D of the exit as $D^{5/2}$ for three-dimensional hoppers. It is also concluded that the flow rate depends on the hopper angle θ as $\sin^{1/2}\theta$ which is consistent with experiments. On the other hand, the prediction of the dependency of flow rate on the neck diameter fails when the diameter is less than six times the diameter of the particles.

To solve the governing equations of the hourglass flow, the HGT borrows from the Free Fall Arch Concept (FFAC): there is a spherical free-fall arch where the radial stress vanishes; below the free-fall arch, the particles lose contact and accelerate freely by gravity [15]. Based on this concept, the Free-Fall Arch Theory (FFAT) has been developed [11, 16]. Recent micromechanical observations of the forces and displacement of the grains near the exit provide some corrections to this FFAC: particle image velocimetry analysis on the flow of bunkers (flat-bottom silos) shows self-similarity in both density and velocity profiles [11]. The analysis of the velocity profile with the FFAC suggests that the arch is not perfectly spherical but rather parabolic [11]. In more recent work, a detailed micromechanical analysis of the stress field concludes that there is not an arch region where the normal stress vanishes [16]. Instead, the free-fall arch is a parabolic curve where the kinetic stress peaks, while the self-similarity of the fields is fully justified.

In this paper, we investigate the self-similarity of the density and velocity profiles in hoppers (silos where walls converge towards exit). Using discrete element simulations of hopper flow, we recover self-similar profiles, although the observed arches are different from the ones in bunker flow [11]. The flow rate resulting from these profiles provides some corrections to the Beverloo relation near the clogging point. We propose a modification of the FFAC based on the assumption that the arch has non-zero velocity at the beginning of free fall. The grain scale kinematic analysis provides a solid interpretation of the parameters used in this relation.

This paper is organized as follows: Sect. 2 presents the dimensional analysis and the numerical method used in this investigation. Section 3 reviews the hourglass theory using

✉ Fernando Alonso-Marroquin
fernando@sydney.edu.au

[1] School of Civil Engineering, The University of Sydney, Sydney, NSW 2006, Australia

[2] College of Petroleum Engineering and Geosciences, King Fahd University of Petroleum and Minerals, Dhahran 31261, Saudi Arabia

numerical simulations. In Sects. 4 and 5 the self-similar density and velocity profiles are calculated, and they are used in Sect. 6 to obtain the Beverloo relations. Conclusions are presented in Sect. 7.

2 Analyses

We will focus on the mass flow rate in a two-dimensional hopper. The mass flow rate W is a function of the width of the neck D, particle diameter d, the half-angle of the hopper θ, the gravity g, and the two bulk properties of the particulate material: bulk density ρ_b and coefficient of friction μ.

If one ignores the effect of particle size, dimensional analysis [15] leads to the simplest law

$$W_{da.} = C(\mu,\theta)\rho_b\sqrt{g}D^{3/2}. \tag{1}$$

The Beverloo relation has been proposed [14] as an empirical formula that accounts for the particle diameter

$$W_{Bev.} = C(\mu,\theta)\rho_b\sqrt{g}(D-kd)^{3/2}. \tag{2}$$

We aim to use micromechanical data to derive a more general law that includes particle size and provides a physical meaning of the parameters used. The observations are taken from simulations of circular particles in an hourglass-shaped hopper. The particles flow through the bottleneck due to gravity and the hopper is refilled using periodic boundary conditions. Error bars are calculated from four random samples. The interaction between particles includes elastic and viscous forces with a Blendel & Dippel sliding condition [5] already implemented for granular dynamic simulations [3].

The parameters of the contact model are: normal and tangential contact stiffness k_n [N/m] and k_t [N/m], friction coefficient μ, and normal and tangential coefficients of viscosity γ_n [s^{-1}] and γ_t [s^{-1}]. The system parameters are particle density of ρ_p [kg/m^2], mean particle diameter d [m]. The driven acceleration is g [m/s^2]. The mass flow rate depends on the above parameters, as well as the half angle of the hopper θ and the neck diameter D. Using the standard method of dimensional analysis [7], we obtain the expression of the mass flow rate:

$$W/W_0 = f(\mu,\theta,D/d,q,a,\kappa), \tag{3}$$

where $W_0 = m(g/d)^{1/2}$, and the dimensionless input variables are the quality factor $q = \omega_0/\gamma_n$, stiffness ratio $a = k_t/k_n = \gamma_t/\gamma_n$, and overlap ratio $\kappa = m\omega_0/W_0$, where $\omega_0 = (k_n/m)^{1/2}$ is the natural frequency at the contact and m is the particle mass. The overlap ratio should be low enough to allow time steps large enough for fast simulation, but high enough to avoid unrealistic overlap; the quality factor is chosen to achieve a mild coefficient of restitution.

The required set of the dimensional parameters to achieve a desired set of dimensionless parameters is not unique. Here the dimensional contact parameters have been tailored to achieve the desired balance between computational efficiency and realistic interactions. The chosen dimensional parameters of the contact model are: normal and tangential contact stiffness $k_n = 1\times10^6$ N/m and $k_t = 1\times10^5$ N/m, friction coefficient $\mu = 0.2$, and normal and tangential coefficients of viscosity $\gamma_n = 100\,s^{-1}$ and $\gamma_t = 10\,s^{-1}$. The values of the system parameters are particle density of $\rho_p = 100\,kg/m^2$ and mean particle diameter $d = 0.3$ m. These parameters lead to $q = 3.76$ that gives a restitution coefficient of 0.42 [4]; $a = 0.1$ leads to a Poisson ratio of 0.3 for hexagonal packing [20]; overlap ratio $\kappa = 0.005$ guarantees overlaps lower than 5% of the particle diameter. The driven acceleration is $g = 1\,m/s^2$ that corresponds to an experimental setup where the particles roll over a surface tilted by 5.7°. The neck is varied between $D = 0.5$ m and 4 m and the hopper half angle is fixed to $\theta = 30°$. Each simulation runs for $34000t_c$, where $t_c = 2\pi/\omega_0$ is the characteristic collision time. The system consists of particles with diameters randomly generated between $0.93d$ and $1.06d$, the number of particles is $N = 3670$, which is enough to guarantee steady flow and a filling height larger than three times the neck diameter so that we can neglect the dependency of flow rate on filling height.

3 Hourglass theory

The main assumptions used by the HGT to predict the flow rate are: (1) There exists a circular arc at the bottleneck where radial stress vanishes; (2) The velocity is radial and independent of angular position; (3) the bulk density is homogeneous in the hopper.

An analytical solution for the mass flowrate has been presented by applying the HGT to narrow conical hoppers with frictionless walls [15]. We present here the derivation for narrow two-dimensional hoppers. The assumption on the narrow hopper is $\tan\phi \approx \phi$ if $|\phi| < \theta$. For our case we have $\theta = 30°$ so that the approximation is valid within an maximal error of 10%.

If the hopper's walls are frictionless, the shear stress vanishes. We use a cylindrical coordinate system (r,ϕ) centered in the apex of the hopper. The radial σ_r and azimuthal σ_ϕ components of the stress are related by

$$\sigma_\phi = K\sigma_r, \tag{4}$$

where K is the earth pressure coefficient. The kinematic equations for the radial v_r and azimuthal v_ϕ components of the velocity are derived from mass conservation and the assumption (2) of the HGT

$$v_r = -V/r, \quad v_\phi = 0. \tag{5}$$

The radial stress and the constant V can be evaluated using the Euler's equation

$$\rho_b v_r \frac{dv_r}{dr} + \frac{d\sigma_r}{dr} + \frac{\sigma_r - \sigma_\phi}{r} + \rho_b g \cos\phi = 0. \tag{6}$$

Using Eqs. (4) and (5) and using the approximation $\cos\phi \approx 1$ for narrow hoppers, this equation reduces to

$$\frac{\rho_b V^2}{r^3} + \frac{d\sigma_r}{dr} + \frac{1-K}{r}\sigma_r + \rho_b g = 0, \tag{7}$$

This ordinary differential equation is solved using the boundary conditions:

$$\sigma_r(r_0) = \sigma_r(r_1) = 0. \tag{8}$$

These conditions state that the bottom ($r = r_0$) and the top ($r = r_1$) of the granulate are free surfaces. The bottom surface is the free-fall arch spanning from the edges of the neck. The solution for V is

$$V^2 = g r_0^3 \frac{1+K}{K-2} \frac{1-(r_1/r_0)^{2-k}}{1-(r_1/r_0)^{-1-k}}. \tag{9}$$

The neck diameter is related to the arch radius by $D/2 = r_0 \sin\theta$. It is assumed that $K > 2$ and the filling height is much larger than the neck diameter so that $r_1 >> r_0$. Then

$$V = \sqrt{\frac{1+K}{2(K-2)}} \frac{g^{1/2} D^{3/2}}{\sin^{3/2}(\theta)}. \tag{10}$$

Replacing this equation into Eq. (5) for $r = r_a$ we obtain an expression for the velocity at the free-fall arch

$$v_{a,HGT} = v_r(r_0) = \sqrt{\frac{1+K}{2(K-2)}} \frac{g^{1/2} D^{3/2}}{\sin^{3/2}(\theta)}. \tag{11}$$

This result can be used to derive the mass flowrate that is calculated by integrating $\rho_p v_r$ over the free-fall arch

$$W_{HGT} = \int_{-\theta}^{\theta} \rho_b v_{a,HGT}(r_a d\phi) = 2\rho_b \theta V. \tag{12}$$

Substituting Eq. (11) into Eq. (12) and using the approximation $\sin\theta \approx \theta$ for narrow hoppers, we obtain an expression for the mass flowrate in terms of neck diameter and hopper angle

$$W_{HGT} = \sqrt{\frac{1+K}{2(K-2)}} \frac{\rho_b g^{1/2} D^{3/2}}{\sin^{1/2}(\theta)} \tag{13}$$

The HGT predicts the dependency of flow rate with the hopper angle by the factor $\sin^{-1/2}\theta$ that agrees with our previous simulations [3]. The flow rate is calculated from a non-zero arch velocity that scales with the neck diameter by $D^{3/2}$ in agreement with experimental data of granular flow when $D >> d$ [11]. For small neck diameters this scaling law fails, and clogging is experienced [15]. Thus, a revision of the HGT is required to achieve a more general flow rate law.

The three main hypotheses of the HGT will be tested by analyzing the data of the interparticle contact network, the velocity field, and the volume fraction of the granular material.

We start testing assumption (1) of the HGT by investigating the contact forces between particles. The contact force network in Fig. 1a is characterized by an intermittent dynamics, due to the creation and destruction of arches above the exit. These arches lead to a strongly fluctuating stress well above the arches, while the material immediately below it is loose, and the stress vanishes. There is

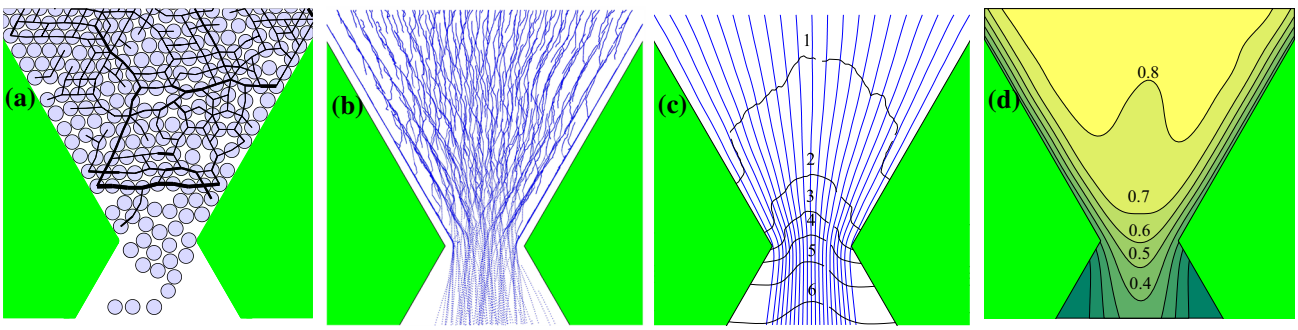

Fig. 1 **a** Contact network of the particles crossing the bottleneck. The thickness of the lines encodes the normal contact forces. **b** Trajectory of the particles. Each dot represents the center of mass of the particle and the dots are superposed for different time steps. **c** The streamlines of the averaged velocity field are obtained as follows: for each time, the velocity is interpolated onto a regular mesh using nearest-neighbor interpolation; then the velocity field is averaged over time at each point of the regular mesh. Finally, the streamlines and the constant-speed lines are obtained from this velocity field. **d** coarse-grained volume ratio taken from Eq. (14) averaged over time.

no evidence of circular arches created at the exit as suggested by the HGT. Instead, the arches are created above the exit and they come in different shapes and sizes. This observation is consistent with the analysis of the stresses by Rubio-Largo et al. [16] that show that the kinetic stress, when averaged over different time stamps, is a monotonic function of the height. However, their observation does not rule out the existence of free-fall arches that occur intermittently during the time.

The existence of free-fall arches is also supported by observations on the kinematics of the particles. In Fig. 1b we track the displacement of the particles. Well above the exit the particles organize in layers parallel to the hopper walls; the thickness of each layer is the diameter of the particles. When the layers collide above the exit, free-fall arches are created (Fig. 1a). When the arches break the particles are driven by gravity with little interaction between them.

Now we test assumption (2) of the HGT. Note that the HGT assumes that the velocity of the particles is radial before the free-fall arch, while the FFAT assumes that the particles just fall vertically due to gravity after the free-fall arch. To test these hypotheses, we plot in Fig. 1c the streamlines and the lines of constant speed from the time-average of the velocity field. In agreement with the HGT, the streamlines are radial well above the exit, but near to the exit they curve so that they become perpendicular to the exit as the FFAT states. We also note that the velocity field in Fig. 1c does not show any arch region where particles lose all kinetic energy and start free falling by gravity. To achieve consistency between both theories we need to depart from the classical FFAT assumption that the particles in the arch start with zero velocity.

From Fig. 1c we note that the lines of constant speed are not perpendicular to the streamlines, suggesting that the flow is compressible, i.e. bulk density is not homogeneous. This observation rules out the assumption (3) of the HGT. To investigate how the volume fraction changes as the particles approach the exit, we calculate the *coarse-grained* volume fraction as proposed by Goldhirsch [9],

$$\boldsymbol{\Phi}(\mathbf{r}) = \pi r^2 \sum_{i=1}^{N} \phi(\mathbf{r} - \mathbf{r}_i), \tag{14}$$

where N is the number of particles, $\mathbf{r}_i$ is the position of the $i-$particle, and $\phi(\mathbf{r})$ is a Gaussian with variance d. The coarse-grained velocity can be calculated as $\mathbf{v}(\mathbf{r}) = (\pi r^2/\boldsymbol{\Phi}(\mathbf{r})) \sum_{i=1}^{N} m_i \mathbf{v}_i \phi(\mathbf{r} - \mathbf{r}_i)$, which is the ratio between momentum and density. This calculation produces large errors near the walls where density vanishes. For this reason, we implement an alternative calculation of the velocity by nearest neighbor interpolation. For alternative methods to deal with coarse-grained calculations near boundaries, see the paper of Weinhart et al [21].

The distribution of the volume ratio is shown in Fig. 1d. Well above the exit the volume fraction is above 0.83, which corresponds to the jamming threshold [13]. The volume fraction is reduced near the hopper walls as no particle can approach the wall closer than its radial distance. But this is not the main factor for the reduction of density; as the particles approach the exit the volume fraction decreases. This is consistent with the loosening of the packing when the arches break. Thus, an extension of the HGT must consider both bulk density and particle velocity as field variables to be solved using mass and moment conservation equations. As an alternative approach, we investigate the density and velocity profiles at the neck and use the FFAT to construct self-similar profiles and to interpret the resulting mass flow relation.

4 Density profiles

If we assume that the span at which the free-fall arch breaks scales as D, then the density profile should also scale with D. To test this hypothesis, we plot the profile of volume fraction along the exit for different apertures in Fig. 2a. When the profiles are rescaled with the exit radius $R = D/2$, all of them collapse into the same curve as shown in Fig. 2b:

$$\boldsymbol{\Phi}(x) = \boldsymbol{\Phi}_c (1 - (x/R)^2)^{1/\nu}, \tag{15}$$

where $1/\nu = 0.2 \pm 0.02$ and the factor $\boldsymbol{\Phi}_c$ depends on the radius as shown the Fig. 2c. The data suggests an exponential saturation for large apertures that can be fitted by the Janda's equation for bunker flow [11].

$$\boldsymbol{\Phi}_c = \boldsymbol{\Phi}_\infty (1 - \alpha_1 e^{-\frac{D}{d\alpha_2}}). \tag{16}$$

The fitted parameters are shown in Table 1. It is interesting that the parameters are very close to the ones obtained by recent experiments and simulations on bunker flow [11, 22]. This consistency may suggest that the self-similar density profile is either universal or it does not depend on the details such as the geometry of the bottleneck or the way the clogging may be prevented.

5 Velocity profiles

Now we analyze the velocity profiles for different outlet widths shown in Fig. 3. Similar to the experiments on bunker flow [11], the shape of the profile does not depend on bottleneck width. Yet there are subtle differences in the observed profile: In bunker flow, the velocity profiles are assumed to reach zero at the edges of the exit, while our profiles reach a finite value that scales with the bottleneck width. Also, the

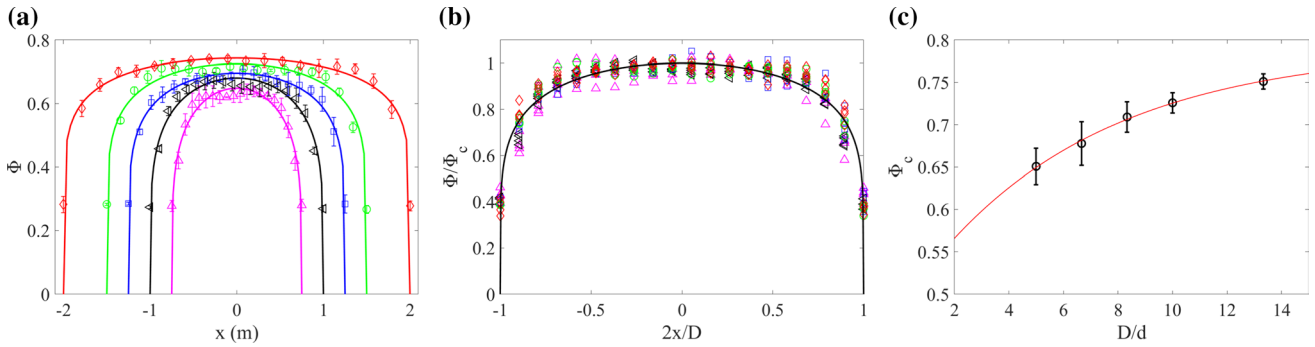

Fig. 2 **a** Volume fraction versus position at the exit for different apertures. The solid lines are the curve fits using Eq. (15). **b** Normalized volume fraction versus normalized position. The solid line is $y(x) = (1 - x^2)^5$ (**c**) Maximal volume fraction versus aperture, the solid line represents the exponential fit, Eq. (16)

Table 1 Fitting parameter of density profile from our hopper flow simulation, and comparison with experiments [11] and simulations [22] of granular bunker flow. The volume fraction is retrieved from [22] assuming the bulk volume ratio of the hexagonal disk packing of 0.9

Parameter	Hopper flow	Bunker flow experiments	Bunker flow simulations
$1/\nu$	0.20 ± 0.02	0.22	0.19 ± 0.1
Φ_∞	0.79 ± 0.01	0.83 ± 0.01	0.80
α_1	0.39 ± 0.004	0.50 ± 0.01	0.45
α_2	6.45 ± 0.5	6.6 ± 0.1	7.7

slope of our velocity profiles is slightly reduced at the edges, which may be related to the effect of the particles that roll over the hopper before exiting. In spite of these differences, our profiles can still be approximated by parabolic profiles.

To interpret the self-similar profiles of the velocity, we propose slight modifications to the FFAT based on two physical arguments: (1) The assumption of a free-fall arch with parabolic shape and non-zero initial velocity, (2) The presumption that particles do not dissipate mechanical energy after the arch breaks. We introduce the free-fall arch as a function $y(x)$ shown in Fig. 4. While the HGT suggests that the arch has circular shape, we assume that the arch has a parabolic shape, which is similar to the experimental observation of Janda et. al. on granular flow [11].

$$y(x) = y_0 - h(x/R)^2, \tag{17}$$

where $R = D/2$ is half of the neck diameter and y_0 and h account for the position and the height of the arch as shown in Fig. 4. We adopt the previous observation that the streamlines enter perpendicular to the edges so that the velocity of the particles exiting the exit is almost vertical. We also consider that the velocity at the arch is non-zero before it breaks. The mechanical energy of the particle with mass m in the arch is $\frac{1}{2}mv_a^2 + mgy(x)$ where v_a is the arch velocity that is assumed to be constant along the arch. The mechanical energy of the same particle when it crosses the neck is $\frac{1}{2}m[v(x)]^2$. Now we assume that in the region between the arch and the exit, the particles either roll over the hopper

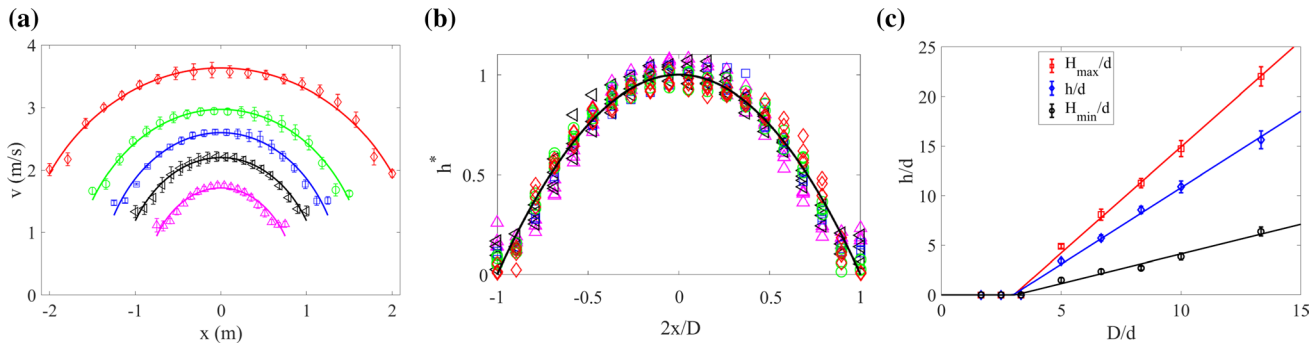

Fig. 3 **a** Velocity versus position at the exit for different apertures. The solid lines are the curve fits using Eqs. (19) and (20). **b** Normalized head of the arch versus normalized position. The normalized head is defined as $h^* = (H - H_{min})/h$, where $H = v^2/(2g)$ and H_{min} and h are the best fits using Eq. (20). The self-similar profile (solid line) is $h^*(x) = 1 - x^2$. **c** Arch descriptors versus neck width. The solid lines represent the best linear fit of H_{min}, h, and $H_{max} = H_{min} + h$ using Eq. (21)

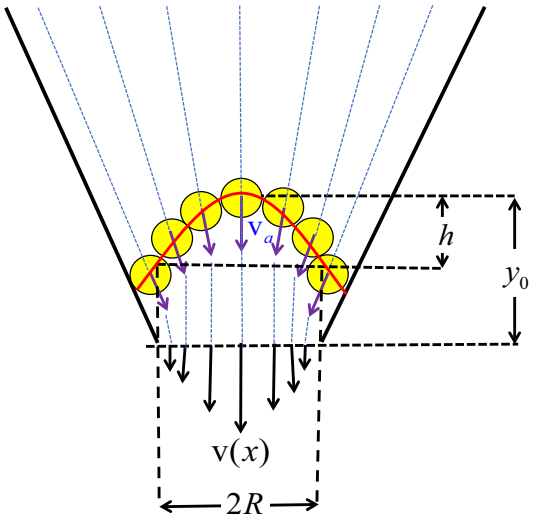

Fig. 4 The free-fall arch is approximated by a parabolic shape $y(x) = y_0 - h(x/R)^2$ where $R = D/2$. The scalar quantity v_a is the initial radial velocity of the arch and the scalar function $v(x)$ is the vertical velocity at the neck

or experience free fall so that the energy dissipation is negligible there. Then the velocity of the particle at the exit is calculated using energy conservation:

$$\frac{1}{2}m[v(x)]^2 = \frac{1}{2}mv_a^2 + mgy(x). \tag{18}$$

For the sake of simplification of the analysis and comparison with previous work on bunker flow [11], we introduce the fluid dynamics concept of kinetic head:

$$H(x) = \frac{[v(x)]^2}{2g}. \tag{19}$$

This quantity will be decomposed to account for both arch height and arch velocity on the velocity profile at the neck as follows: Replacing Eqs. (17) and (18) into this equation we obtain the kinetic head at the neck:

$$H(x) = H_{min} + h[1 - (x/R)^2], \tag{20}$$

where $H_{min} = h_a + h_{min}$ is the kinetic head at the end of the neck that is the sum of the kinetic head due to the elevation of the arch $h_{min} = y_0 - h$ and the kinetic head due to the initial velocity of the arch $h_a = v_a/(2g)$. Note that at the ends of the neck ($x = R$), the minimal kinetic head is $H = H_{min}$ and hence, due to Eq. (19), the velocity at the ends of the neck is not necessarily zero. Non-zero velocities at the end of the neck are also observed in the granular flow experiments of Janda et al. [11] but they are small and can be neglected for bunker flow. In our simulations of hopper flow, the velocity at the ends is not negligible and we need to take this into account. This necessitates an increase in the number of fitting parameters of our model.

We use Eq. (20) to construct self-similar profiles of the normalised kinetic head $h^* = (H - H_{min})/h$ that collapse to the curve $h^*(x) = 1 - x^2$, see Fig. 3b. Figure 3c shows an excellent fit for the dependency of H_{min} and h on bottleneck width that is given by

$$\frac{H_{min}}{\gamma_m} = \frac{h}{\gamma} = \Theta(D - kd), \tag{21}$$

where the ramp function is defined as $\Theta(x) = x$ if $x > 0$ or zero otherwise. The fitting parameters are $\gamma_m = 0.6 \pm 0.1$, $\gamma = 1.54 \pm 0.1$ and $k = 3.0 \pm 0.2$. This contrasts to the single fitting parameter $\gamma = 1.07$ required in bunker flow analysis [11]. The height of the arches is a linear relation with the diameter shifted by kd. The factor k appears also in the Beverloo relation to describe the shift of the power-law relation between mass flow rate and the neck width [15]. In the HGT, this shift is mistakenly attributed to the effect of the *empty annulus* – a hypothetical region near the edges of the exit where the density, and hence the flow rate is strongly reduced [6]. In contradiction to this hypothesis, the parameter k in our simulations is directly related to the velocity field and not the density profile. In our simulations, we need a minimum of three particles to create a metastable free-fall arch that can be broken by the agitation of the incoming particles. If the diameter of the exit is smaller than three-particle diameters, highly stable arches are eventually created and therefore the velocity is vanishingly small. However, this variable should not be related to a clogging transition. As in the concept of empty annulus, the existence of a clogging transition is still debatable in the literature. In our paper, the onset of clogging is at three-particle diameters, while other papers report clogging at 6–8 particle diameters. Clogging depends on the nature of the contact interaction, and in particular on the friction coefficient [19]. Clogging also appears at higher neck widths for non-convex particles [2]. Besides, detailed experimental observations prove that there is not sharp clogging transitions but all hoppers have a non-zero probability to clog [17, 18].

Let us compare our results with experiments on granular bunker flow. The original FFAT assumes that the arch is spherical with no initial velocity, thus $H_{min} = 0$ and $h = R$. Experiments on granular bunker flow proposed a correction of the parabolic arch so that $h = \gamma R$ with $\gamma = 1.07$ [11]. From Eq. (21) we obtain a non-zero $H_{min} = \gamma_m(R - kr)$ where r is the particle radius. In addition, the height of the arch is corrected by $h = \gamma(R - kr)$. The fitted value of $\gamma = 1.54$ indicates that the deviation from the spherical arch shape is of 54% – much larger than the 7% deviation from bunker flow. The main results from the classical and modified FFAT analysis are presented in Table 2.

Table 2 Comparison of results for kinetic head and velocity from different FFAT models

Model	h	H_{max}	$v(0)$	$v(R)$
Classical [15]	R	0	$\sqrt{2gR}$	0
Janda et al. [11]	γR	0	$\sqrt{2\gamma gR}$	0
This paper	$\gamma\xi(R)$	$\gamma_m\xi(R)$	$\sqrt{2\gamma g\xi(R)}$	$\sqrt{2\gamma_m g\xi(R)}$

The last one is our model where $\xi(R) = \theta(R - kr)$

6 Beverloo relation

Now we will use the above results to construct the modified Beverloo formula for flow rate. Since the flow is stationary, the mass flow rate is obtained by integrating over the neck

$$W = \int_{-D/2}^{D/2} \rho_p \boldsymbol{\Phi}(x) v(x) dx. \tag{22}$$

The volume fraction $\boldsymbol{\Phi}$ is calculated from Eqs. (15) and (16) and the velocity profile v results from the Eqs. (19), (20) and (21):

$$\begin{aligned} \boldsymbol{\Phi}(x) &= \boldsymbol{\Phi}_\infty(1 - \alpha_1 e^{-D/d\alpha_2})(1 - (x/R)^2)^{1/\nu}, \\ v(x) &= [2g\Theta(D - kd)(\gamma_m + \gamma(x/R)^2)]^{1/2}. \end{aligned} \tag{23}$$

Replacing Eqs. (23) and into (22) we obtain the expression for the mass flow rate for $D > kd$:

$$W = C\rho_b(D)\sqrt{g}D(D - kd)^{1/2}, \tag{24}$$

where $C = \sqrt{2}\int_0^1 (1 - t^2)^{1/\nu}(\gamma_m + \gamma t^2)^{1/2} dt$ and the bulk density is given by $\rho_b(D) = \rho_p \boldsymbol{\Phi}_\infty(1 - \alpha_1 e^{-\frac{D}{d\alpha_2}})$. Our flow rate equation is similar to the Beverloo relation given by Eq. (2). Both equations are applicable for $D \leq kd$ and zero flow rate is assumed when $D < kd$. In the limit $D/d \to \infty$, both equations converge to the equation derived from dimensional analysis (Eq. (1)).

Figure 5 shows the numerical data and the best fits using the three models. The flow rate is first calculated from the simulations by counting the particles crossing the periodic boundary conditions. The data is then fitted with our model given by Eq. (24) and the Beverloo model given by Eq. (2). Both models provide a reasonable fit to the data but there are subtle differences: While the Beverloo curve is smooth, our curve has a discontinuity in the derivative of the flow rate at $D = kd$. This discontinuity defines the critical neck width below which the particles start clogging. While the Beverloo relation is fully empirical, the parameters of our model can be interpreted from the self-similar density and velocity profile.

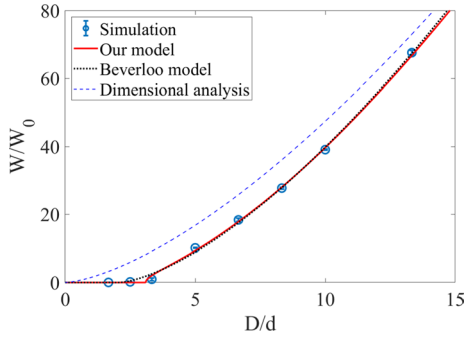

Fig. 5 Mass flow rate versus neck width and best fit with the Beverloo relation, our model, and dimensional analysis. The normalizing factor is $W_0 = m(g/d)^{1/2}$

7 Conclusions

We derived the Beverloo relation for hopper flow from self-similar velocity and density profiles. The self-similar analysis proved to be valid from both bunker flow and hopper flow. The density profiles seem to obey a universal law in both cases, and the kinetic head profile can be reasonably adjusted to a parabolic profile. The velocity profile is calculated in terms of the position, velocity, and height of the free-fall arch. We extend the classical FFAT theory by introducing a correction that accounts for the initial velocity of the arch and the position of the base of the arch.

The new Beverloo relation is constructed based on three physical arguments: (1) The existence of a universal self-similar density profile, (2) the presumption of a free-fall arch with a parabolic shape and non-zero initial velocity, and (3) the assumption that the particles convey to the exit with negligible dissipation after the arch breaks.The analysis of the velocity profiles is characterized by three parameters γ, γ_m, and k. This contrasts with the single parameter γ used in bunker flow. This is reasonable since the hopper flow has two additional parameters: the hopper angle as a geometric parameter, and the particle-wall friction as a material parameter.

Including a robust Beverloo relation for the mass flow requires an in-depth revision of the HGT and FFAT based on a larger set of numerical and experimental data that should include the effect of hopper angle, particle polydispersity, and particle shape. We anticipate that increasing polydispersity will remove the effect of crystallization, and varying the friction coefficient, hopper angle, and particle shape may lead to different flow regimes.

Compliance with ethical standards

Conflict of interest The authors declare that they have not conflict of interest.

References

1. Aguirre, M.A., Grande, J.G., Calvo, A., Pugnaloni, A.L., Géminard, J.-C.: Granular flow through an aperture: pressure and flow rate are independent. Phys. Rev. E **83**(6), 061305 (2011)
2. Alonso-Marroquin, F.: Spheropolygons: a new method to simulate conservative and dissipative interactions between 2d complex-shaped rigid bodies. Europhys. Lett. **83**(1), 14001 (2008)
3. Alonso-Marroquin, F., Azeezullah, S.I., Galindo-Torres, S.A., Olsen-Kettle, L.M.: Bottlenecks in granular flow: when does an obstacle increase the flow rate in an hourglass? Phys. Rev. E **85**(2), 020301 (2012)
4. Alonso-Marroquin, F., Ramirez-Gomez, A., Gonzalez-Montellano, C., Balaam, N., Hanaor, D.A.H., Flores-Johnson, E.A., Gan, Y., Chen, S., Shen, L.: Experimental and numerical determination of mechanical properties of polygonal wood particles and their flow analysis in silos. Granular Matter **15**(6), 811–826 (2013)
5. Brendel, L., and Dippel, S. Lasting contacts in molecular dynamics simulations. In; Physics of Dry Granular Media, pp. 313–318. Springer (1998)
6. Brown, R.L., Richards, J.C.: Kinematics of the flow of dry powders and bulk solids. Rheol. Acta **4**(3), 153–165 (1965)
7. Buckingham, E.: On physically similar systems: illustrations of the use of dimensional equations. Phys. Rev. **4**, 345–376 (1914)
8. Garcimartín, A., Pastor, J.M., Ferrer, L.M., Ramos, J.J., Martín-Gómez, C., Zuriguel, I.: Flow and clogging of a sheep herd passing through a bottleneck. Phys. Rev. E **91**(2), 022808 (2015)
9. Goldhirsch, I.: Stress, stress asymmetry and couple stress: from discrete particles to continuous fields. Granular Matter **12**(3), 239–252 (2010)
10. Haghani, M., Sarvi, M.: Simulating pedestrian flow through narrow exits. Phys. Lett. A **383**(2–3), 110–120 (2019)
11. Janda, A., Zuriguel, I., Maza, D.: Flow rate of particles through apertures obtained from self-similar density and velocity profiles. Phys. Rev. Lett. **108**(24), 248001 (2012)
12. Kondic, L.: Simulations of two dimensional hopper flow. Granular Matter **16**(2), 235–242 (2014)
13. Majmudar, T.S., Sperl, M., Luding, S., Behringer, P.R.: Jamming transition in granular systems. Phys. Rev. Lett. **98**(5), 058001 (2007)
14. Mankoc, C., Janda, A., Arevalo, R., Pastor, J.M., Zuriguel, I., Garcimartín, A., Maza, D.: The flow rate of granular materials through an orifice. Granular Matter **9**(6), 407–414 (2007)
15. Ronald Midgley Nedderman: Statics and Kinematics of Granular Materials, Chapter 10. Cambridge University Press, Cambridge (2005)
16. Rubio-Largo, S.M., Janda, A., Maza, D., Zuriguel, I., Hidalgo, R.C.: Disentangling the free-fall arch paradox in silo discharge. Phys. Rev. Lett. **114**(23), 238002 (2015)
17. Thomas, C.C., Durian, J.D.: Fraction of clogging configurations sampled by granular hopper flow. Phys. Rev. Lett. **114**(17), 178001 (2015)
18. To, K.: Jamming transition in two-dimensional hoppers and silos. Phys. Rev. E **71**(6), 060301 (2005)
19. To, K., Lai, P.-Y., Pak, H.K.: Jamming of granular flow in a two-dimensional hopper. Phys. Rev. Lett. **86**(1), 71 (2001)
20. Wang, Y., Mora, P.: Macroscopic elastic properties of regular lattices. J. Mech. Phys. Solids **56**(12), 3459–3474 (2008)
21. Weinhart, T., Thornton, R.A., Luding, S., Bokhove, O.: From discrete particles to continuum fields near a boundary. Granular Matter **14**(2), 289–294 (2012)
22. Zhou, Y., Ruyer, P., Aussillous, P.: Discharge flow of a bidisperse granular media from a silo: discrete particle simulations. Phys. Rev. E **92**(6), 062204 (2015)
23. Zuriguel, I., Parisi, D.R., Hidalgo, R.C., Lozano, C., Janda, A., Gago, P.A., Peralta, J.P., Ferrer, L.M., Pugnaloni, L.A., Clément, E., et al.: Clogging transition of many-particle systems flowing through bottlenecks. Sci. Rep. **4**, 7324 (2014)